Lignin-based Mucin-mimicking Antiviral Hydrogels with Enzyme Stability and Tunable Porosity

Sanjam Chandna[a]*, Tatyana L. Povolotsky[a], Chuanxiong Nie[a], Stefanie Wedepohl[a], Elisa Quaas[a], Kai Ludwig[a], Yulia Boyakova[a], Sumati Bhatia[c], Klas Meyer[b], Jana Falkenhagen[b], Rainer Haag[a], Stephan Block[a]*

a Institute for Chemistry and Biochemistry, Freie Universität Berlin, Germany

b Federal Institute for Materials Research and Testing (Bundesanstalt für Materialforschung und -prüfung), Berlin, Germany

c Department of Chemistry, Swansea University, UK

Abstract

Mucus is a complex hydrogel acting as a defensive and protective barrier in various parts of the human body. The structure and composition of mucus play an important role in maintaining barrier properties by acting as a filter for the diffusion of biomolecules and pathogens. The rise in viral infections has underscored the importance of advancing research into mucus-mimicking hydrogels for the efficient design of antiviral agents. However, the performance of an antiviral strategy should not only be assessed based on its efficacy in inhibiting infections but also based on its sustainability. Herein, we demonstrate the gram-scale synthesis of biocompatible, lignin-based virus-binding inhibitors that reduce waste and ensure long-term availability. The lignin-based inhibitors were equipped with sulfate moieties, which are known binding partners for many viruses including SARS-CoV-2 and herpes viruses. In addition, crosslinking the synthesized inhibitors yielded hydrogels that mimicked native mucus with respect to surface functionality and rheology. It is found that the degree of sulfation has a very strong impact on the mesh size distribution of the hydrogels, which provides a new means to fine-tune steric and electrostatic contributions of the virus-hydrogel interaction. This feature strongly impacts the sequestration capability of the lignin-based hydrogels, which is demonstrated by infection inhibition assays involving human herpes simplex virus-1, influenza A viruses, and the bacterium *Escherichia coli (E. coli)*. For HSV-1 and *E. coli*, these measurements showed a reduction in plaque (HSV-1) and colony-forming units (*E. coli*) by more than 4 orders of magnitude, indicating potent inhibition by the lignin-based hydrogels. Taken together, the sulfated lignin hydrogel is an excellent scaffold for large-scale synthesis of sustainable, biocompatible, and highly efficient pathogen-binding inhibitors.

Introduction:

Hydrogels are three-dimensional networks of hydrophilic polymers that can absorb and retain large amounts of water or biological fluids while maintaining their structural integrity.[1, 2] Mucus hydrogels that line biointerfaces play a vital role in both shielding the body from invading pathogens and facilitating the proper functioning of the underlying cells.[3] Mucus forms the first line of defense for protecting epithelial cells by acting as a physical barrier for the passage of deleterious molecules.[4] It allows the entry of nutrients and other vital molecules, but protects our body from pathogens such as certain dangerous viruses and bacteria.[5] The majority of mucus consists of water (~95% w/w), and the rest is composed of mucins, globular proteins, salts, lipids, DNA, and cellular debris.[6] Variable mesh size distribution is an important parameter for mucus hydrogels in order to bind the particles of interest, according to their size distribution.[7] The pore size of mucus hydrogels *in vivo* lies in the range of a few hundred nanometers, excluding larger objects such as bacteria and yeast cells.[6] Objects less than the pore size, such as viruses, are caught in the mucin network by sticking to the highly glycosylated structures in the mucosa and are removed from the body.[8] Hence, along with acting as a barrier by affinity sorting, the mucus gels play the role of a filter.[9] These properties inspired the development of mucin-mimicking macromolecules and mucus-mimicking hydrogels, which inhibit infections by forming barriers to pathogens, such as viruses.[10, 11]

To reduce the carbon footprint involved in the synthesis of such compounds, we aimed for a synthesis strategy that employs materials originating from natural sources and evaluated the possibility of forming mucin-mimicking macromolecules using lignin. Lignin comes up as an almost endless raw material produced through photosynthesis, which is currently significantly underutilized.[12, 13] As the second most abundant organic compound on earth, it is one of the main components of biomass which is thrown away in large quantities (approximately 70 Mio tons/year) as a by-product of paper and pulp industries.[14, 15] It has an irregular 3D structure, which is mainly built from three subunits, *i.e.*, guaiacyl (G), p-hydroxyphenyl (H), and syringyl (S). [1, 16-23] The complex organic structure of lignin provides this polymer with valuable properties, such as antioxidant, adhesiveness, UV-barrier, and antimicrobial properties. Owing to its highly diverse structure, good biocompatibility, and abundance in nature, lignin has the potential for biological applications and becomes a sustainable choice for the development of hydrogels in this work.[24] Lignin and lignin-based hydrogels have been explored for different applications in literature due to the fascinating chemistry of lignin, decorated with numerous polyphenolic groups.[22, 25-27] An interesting avenue is the development of antiviral materials through functionalization of lignin.

As many viruses carry a net charge on their surface (caused by the presence of specific proteins or glycoproteins),[28] by modulating the hydrogel's charge density it is possible to create attractive or repulsive forces acting between virus and hydrogel, leading to virus binding or repulsion, respectively. For instance, herpes simplex virus type 1 (HSV-1), a pervasive pathogen responsible for oral and genital herpes, relies on host cell surface interactions mediated by heparan sulfates (a class of sulfated carbohydrates) during its initial stages of infection.[29-31] It utilizes electrostatic interactions to bind with the heparan sulfates present on the cell surface to initiate infection.[31,32] Heparan sulfates make up the outermost part of the cell membrane and the extracellular matrix. [30, 33] Therefore, development of sulfated polymeric inhibitors with high binding affinity to Herpes simplex virus is highly motivating for this work.

This work attempts to design mucus-mimicking hydrogels using lignin as the starting material, by modulating the charge, functionalities, rheological parameters and porous network. We

functionalized lignin with a typical viral attachment factor (sulfates), which enables the functionalized lignin to bind efficiently to viruses. Interestingly, after sulfation, lignin was found to be completely soluble in water, enabling to generate lignin-based hydrogels with high binding capacity for viruses. We systematically varied the concentration of lignin in order to tune the pore size and rheological properties of the lignin-based hydrogels. The sulfated lignin hydrogels were highly efficient against HSV-1 and showed excellent results for binding and inactivation of the virus. To analyse the functionalized hydrogels for the broad-spectrum antimicrobial activity, we also attempted to test the binding affinity towards bacteria (*E. coli*). This work aids in the development of highly sustainable and cost-effective infection control strategies to disrupt the interactions between pathogens and mucus. Lignin-based mucin-mimicking hydrogels can also be potentially used to develop coatings for medical devices that prevent viral adhesion to mucosal surfaces.

Results and Discussion:

Concept of the sulfated lignin and hydrogel synthesis: Mucus is a complex aqueous fluid which is made up of smaller proteins, lipids, electrolytes, and the glycoprotein mucin.[4] These components give mucus its viscoelastic, lubricating, and hydrating qualities. Mucus carries negative charges due to the presence of sulfate groups and sialic acid residues on glycoproteins. Such residues typically act as pathogen attachment factors and help in the exclusion of infectious agents from the body through the mucosa linings present in various parts of the body. This inspired us for the functionalization of lignin with sulfate groups ($-SO_3^-$) through the replacement of hydroxyl moieties.[12, 34] To this end, kraft lignin was functionalized with sulfates to generate the sulfated lignin (represented through a chemical scheme in Figure 1). The success of the functionalization was confirmed by ^{31}P NMR (Figure 2, Table 1(supporting information) and elemental analysis (Figure S1 (b), supporting information).

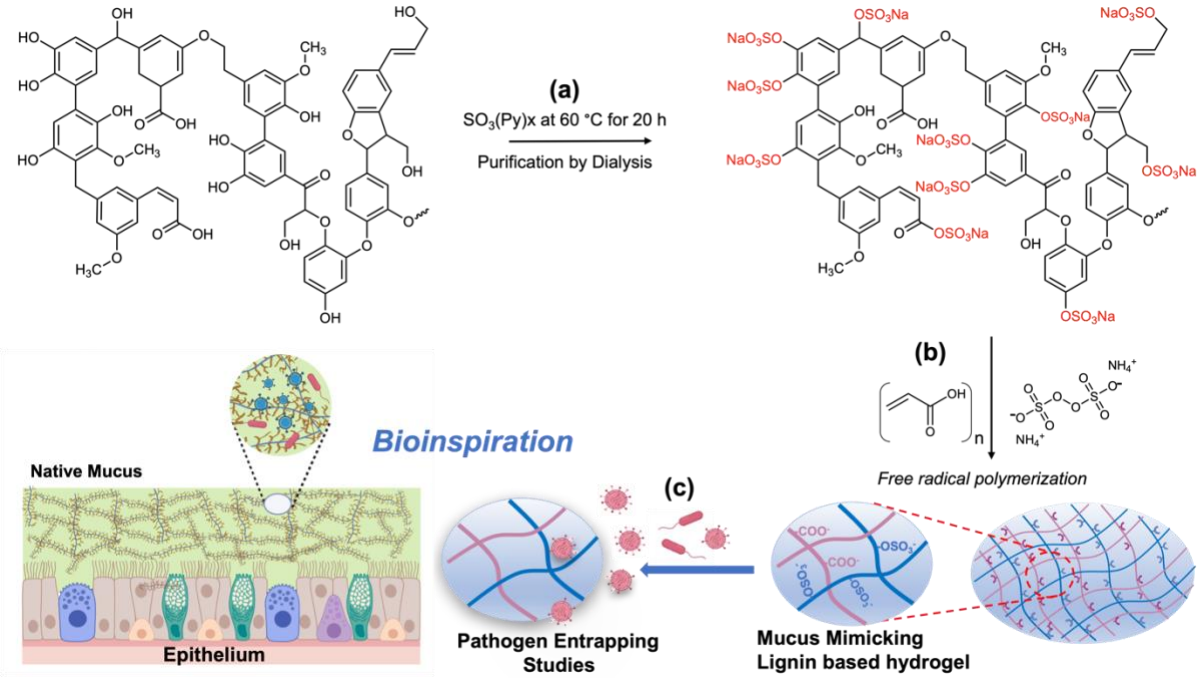

Figure 1. (a) The sulfation process of lignin and (b) subsequent synthesis of lignin-based hydrogels by free radical polymerization at 70°C (c) pathogen entrapping studies of the hydrogel, which is designed to mimic mucus (inspired by native mucus).

For the formation of lignin-based hydrogels, functionalized lignin was copolymerized with polyacrylic acid (PAA) using ammonium persulfate (APS) as a free radical initiator. This facilitates the crosslinking through ester bond formation between the (remaining) -OH bonds of lignin and -COOH bonds of polyacrylic acid, which leads to the formation of a stable hydrogel network (Figure 1 and 2a). Briefly, the lignin acryl ester is formed which is polymerized with acrylic acid to form a hydrogel. The synthesis process was straightforward and simple, which was carried out at 70°C for 30 minutes.

Physical characterization of the functionalized lignin powders: To assess the impact of the degree of sulfation (DoS) on the physicochemical properties of lignin powder, we aimed for sulfated lignin (denoted as SL1 and SL2 in the following), in which approximately half (SL1) or all (SL2) of the available hydroxyl groups have been converted into sulfates. This conversion was monitored based on the ^{31}P NMR chemical shifts in the region of 146 to 148 p.p.m., which correspond to aliphatic hydroxyl groups and show a significant decrease in the cases of SL1 and SL2 (Figure 2a). Moreover, chemical shifts were observed in the region of 137 to 145 p.p.m. corresponding to the phenolic groups in lignin (syringyl, guaiacyl and p-hydroxyphenyl). The amount of aliphatic hydroxyl and phenolic units were calculated in the bare lignin (BL), SL1, and SL2 (summarized in table S1 of the supporting information).[35] The decrease in these groups is paralleled by an increase in sulfates as indicated by elemental analysis (Figure S1 (b), supporting information), which proves successful sulfation of the lignin, leading to DoS values of approximately 78% (SL1) and 90% (SL2).

The sulfation process adds negative charges to lignin, which increases with the degree of sulfation (Figure 2b). The surface charge of the lignin samples was measured through zeta potential analysis, which is a measure of the electrostatic charge at the surface of particles or molecules in a colloidal dispersion. The surface charge influences the stability and behavior of colloidal systems, such as suspensions and emulsions. [36, 37] This addition of negatively charged groups to lignin significantly alters its zeta potential, therefore, the values of zeta potential decrease from -21.9 mV in the case of bare lignin to -35.4 mV (SL1) and -50.2 mV (SL2), respectively (Figure 2a). This addition of negative charges further supports the results from ^{31}P NMR and elemental analysis. It can be hypothesized that the increased negative charge density leads to stronger electrostatic repulsion between sulfated lignin particles. This repulsion prevents them from coming close together and agglomerating, thereby enhancing the stability of colloidal dispersions containing sulfated lignin.

For the determination of the molecular weight distribution of bare and sulfated lignin, size exclusion chromatography (SEC) was performed (Figure S1(a), supporting information). The molecular weight (M_w) of the bare (unmodified) lignin was deduced to be 7300 g/mol. It was observed that the peak in the chromatogram becomes narrower, and the M_w (weight average molar mass) increases upon sulfation to 9540 (SL1) and 8650 g/mol (SL2), respectively. This clearly indicates that the molecular weight distribution of sulfated lignin shifts to larger values and becomes more monodisperse (Figure S1(a), supporting information). These results were further confirmed by the particle size distribution analysis of the lignin samples (Figure S3, supporting information). The values for the size distribution, zeta potential and molecular weight analysis are summarized in Table 1. Further, UV-visible spectroscopy displayed no significant shifts of the absorption maxima of lignin (centered at ~ 280 nm) upon sulfation (Figure S4, supporting information), suggesting that introducing sulfate groups does not

significantly alter the electronic transitions that UV-vis spectroscopy is sensitive to. To gain further insights into the impact of sulfation on the chemical structure of lignin, FTIR spectra of sulfated lignin and bare (unmodified) lignin were determined (Figure S5a, supporting information). A sharp peak was observed between the region of 1200 and 1300 cm^{-1}, which is, in agreement with previous studies, attributed to sulfate groups ($-SO_3H$).[17, 38] There were also peak shifts observed in the CO stretching of lignin from ~ 1020 to ~1100 cm^{-1}. Moreover, a sharpening of the OH peak at ~ 3500 cm^{-1} was observed indicating intramolecular OH bonding.[16, 17, 39]

As mucus is a natural substance in the body, polymers designed to mimic mucus should be biocompatible and safe for use in biological systems without causing harm or triggering an immune response. To investigate the potential of the sulfated lignin polymers, the viability of VeroE6 cells (as a model for fibroblast cells which are also used for virus propagation) was tested after 48 h of exposure (Figure 2c). It was observed that cells exposed to SL1 or SL2 showed no reduction in their viability up to a polymer concentration of 1 mg/mL, indicating a high compatibility with Vero E6 cells. The bare lignin showed a decrease in the cell viability at the concentration of 1 mg/mL, which can be attributed to the effect of DMSO that had to be added to solubilize bare lignin (Figure 2c). The addition of DMSO was not necessary for the sulfated lignin samples, as they were completely soluble in water. Interestingly, the biocompatibility of the sulfated lignin hydrogels increased significantly as compared to the bare lignin.

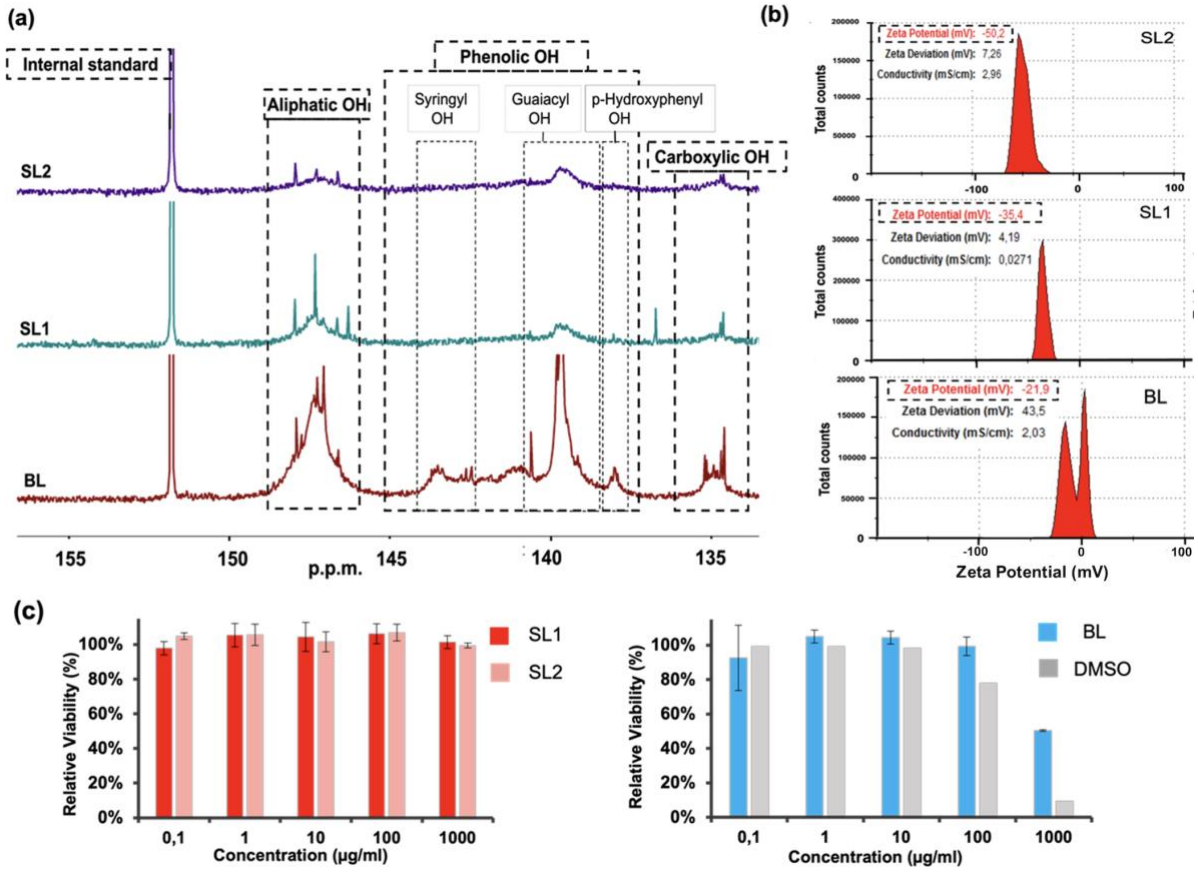

Figure 2. (a) ^{31}P NMR Analysis (b) Analysis of surface charge through zeta potential analysis of bare lignin (BL) as well as the sulfated lignin SL1 and SL2. (c) Relative viability of Vero E6 cells after 48 h of exposure to the compounds as indicated in the legend.

Therefore, it can be concluded that by introducing sulfate moieties onto lignin's intricate macromolecular architecture, the resulting derivatives 1) exhibit improved solubility in aqueous solution, 2) enhanced reactivity, making it more amenable to chemical reactions, such as crosslinking, grafting, and polymerization and 3) increase the biocompatibility of the lignin.

Table 1. Zeta potential, hydrodynamic radius, SEC-determined molecular weight (by SEC) as well as the IC_{50} values for the interaction of the lignin with human herpes simplex virus 1 (HSV-1).

Sample	Degree of Sulfation	Particle Size (nm)	Zeta Potential (mV)	Molecular weight, Mw (g/mol)	IC_{50} values (µg/ml)	IC_{50} values (nM)
BL	-	309 ± 16	-21.9 ± 2.54	7278.6	86.8	$11.9 * 10^3$
SL1	78	216 ± 9.8	-28.7 ± 3.15	9535.5	2.85	298
SL2	90	167 ± 8	-35.4 ± 1.69	8641.3	0.48	55.5

Hydrogel Characterization: Rheology, Enzymatic stability, and Electron Microscopy: After the detailed analysis of the surface characteristics, the bare and sulfated lignins were subjected to hydrogel synthesis. The parameters for the hydrogel synthesis were designed and optimized carefully to mimic the native mucus hydrogels. The high solubility of the sulfated lignin in aqueous medium facilitated the hydrogel synthesis through a sustainable and mild process. Spinnability in hydrogels is their capability of thread-formation arising from non-Newtonian flow. For this, an important prerequisite is the existence of both viscous and elastic properties. Initially, at a lignin concentration of 2 wt%, the hydrogel obtained was rigid and exhibited high viscoelastic properties, and it also did not tend to flow within the measured time period. It is suggested from the results that the synthesized lignin hydrogel is also quite elastic as it shows minimal flow upon pressure application and as pressure is removed, it recoils quickly back to its previous position. However, as the hydrogel concentration decreases from 2 wt % to 0.5 wt% of lignin, it appears to be a viscous hydrogel with high spinnability, maintaining its network structure and elasticity (represented in figure 3a).

As hydrogels are polymeric materials that can swell in water and retain a significant fraction of water within their structure, the swelling rate is one of the most important properties of hydrogels.[40] To measure the swelling rate of sulfated lignin and bare lignin hydrogels, the profile of swelling capacity versus time of the hydrogel samples was obtained by performing free-absorbency capacity measurements at consecutive time intervals. Firstly, the synthesized hydrogels were subjected to freeze drying and then the completely dried hydrogels were kept inside water for swelling. It was deduced that the free swell water retention value (WRV) of the sulfated lignin hydrogel was approximately 1600, which was reduced to ~1454 in the case of bare lignin hydrogels (Figure 3b). However, it can be concluded that both hydrogels exhibit high water absorption abilities. Further details regarding the swelling capacity analysis are also mentioned in the supporting information, figure S8.

The mechanical properties of a substance are indicated by its viscoelastic properties, which can be evaluated through oscillatory rheology experiments. Mucus hydrogels are viscoelastic and sticky, making them effective at trapping and immobilizing foreign particles and pathogens. Viruses, bacteria, and other microorganisms can become entangled in the mucus matrix, preventing them from reaching and infecting the underlying cells. For a hydrogel to mimic native

mucus, it's storage modulus and loss modulus should lie in the range of 1-10 Pa and 0.1 to 1 Pa, respectively.[41, 42] To establish the linear viscoelastic region, the entire frequency series was first subjected to strain-sweep tests and consecutive oscillatory rheology experiments were conducted in this region. The storage modulus and loss modulus were deduced as a function of the radial frequency ω. All the experiments were conducted at 25º C. The rheological behaviour of hydrogels formed using bare lignin (BL-H) or sulfated lignins (SL1-H and SL2-H, respectively) is shown in figure 3c-e and it was speculated that all the synthesized hydrogels exhibited significant elastic-dominant behaviour, therefore proving the stability of the crosslinks. The concentration of lignin during hydrogel formation was optimized to modulate the rheological properties of the developed hydrogel. Varying the concentration of lignin between 0.5% and 2% revealed a significant impact on the elastic and viscous modulus (G' and G", respectively) of the resulting hydrogel (Fig. 3c-e and Table 2). It was observed that upon sulfation of the lignin hydrogels, the storage modulus increased by roughly two orders of magnitude, which indicates an increase in cross-linking density in the sulfated lignin hydrogels. This finding was used to optimize the synthesis parameters to achieve the G' and G" values of the order of native mucus. The synthesized hydrogels were tested for their stability against enzymatic cleavage by the protein hyaluronidase. Hyaluronidase is an enzyme present in synovial fluid, which is responsible for lubrication of joints and acts as a shock absorber. It helps reduce friction between bones and cartilage during joint movement, contributing to joint health and mobility. In order to test the stability of the synthesized hydrogel in presence of hyaluronidase, hydrogels were incubated with the enzyme at 37 °C for 30 hours, followed by evaluation of hydrogel rheology and by measuring changes of storage and loss modulus. It was observed that the viscosity of all the hydrogels (BL-H, SL1-H and SL2-H) was affected by hyaluronidase incubation; however, the hydrogels still maintained storage modulus values between 1 to 10 Pa till the frequency of 5 Hz (Figure 3f, g). Similarly, after enzyme treatment the loss moduli of the BL-H, SL1-H and SL2-H were in the range of 0.1 to 1 Pa, which highly resembles native mucus (Figure 3h). Further incubation of the hydrogels with hyaluronidase did not affect their rheology and physical structure or appearance. This analysis concludes that the synthesized hydrogels are highly stable against enzymatic degradation by natural enzymes, such as hyaluronidase.

Table 2. Storage (G') and loss (G″) modulus values of lignin hydrogels as a function of radial frequency (ω) of 1 Hz at 37 °C

Lignin Concentration	Storage Modulus (Pa) (G')			Loss Modulus (Pa) (G")		
(weight %)	BL-H	SL1-H	SL2-H	BL-H	SL1-H	SL2-H
2	55.56	105.6	229.1	6.6	5.5	6.8
1.5	26.63	45	64.9	2.14	2.2	2.4
1	5.82	17.3	37.8	0.6	1.9	1.52
0.5	0.13	4.9	6.7	0.03	0.8	0.48

In order to gain insights into the surface morphology and internal structure of the hydrogel, the lignin hydrogels were subjected to scanning electron microscopy (SEM) analysis, which provided valuable insights into the surface morphology and partially into the internal structure of the hydrogel (Figure 3i). In the SEM images of SL1-H and SL2-H (1 w/v % lignin), the surface of the sulfated lignin hydrogels appeared to be highly porous (Figure 3i and Figure S7, supporting information), with pore sizes ranging from 800 nm to 2 µm (SL2), 8 to 10 µm (SL1) or being on the order of 25 µm (BL), respectively. This porous morphology clearly resembled the SEM images of native mucus, which was a significant and motivating finding.[5, 43, 44]

Furthermore, the pore size analysis measurements indicated that increasing the DoS caused the pore size distribution to shift towards smaller values.

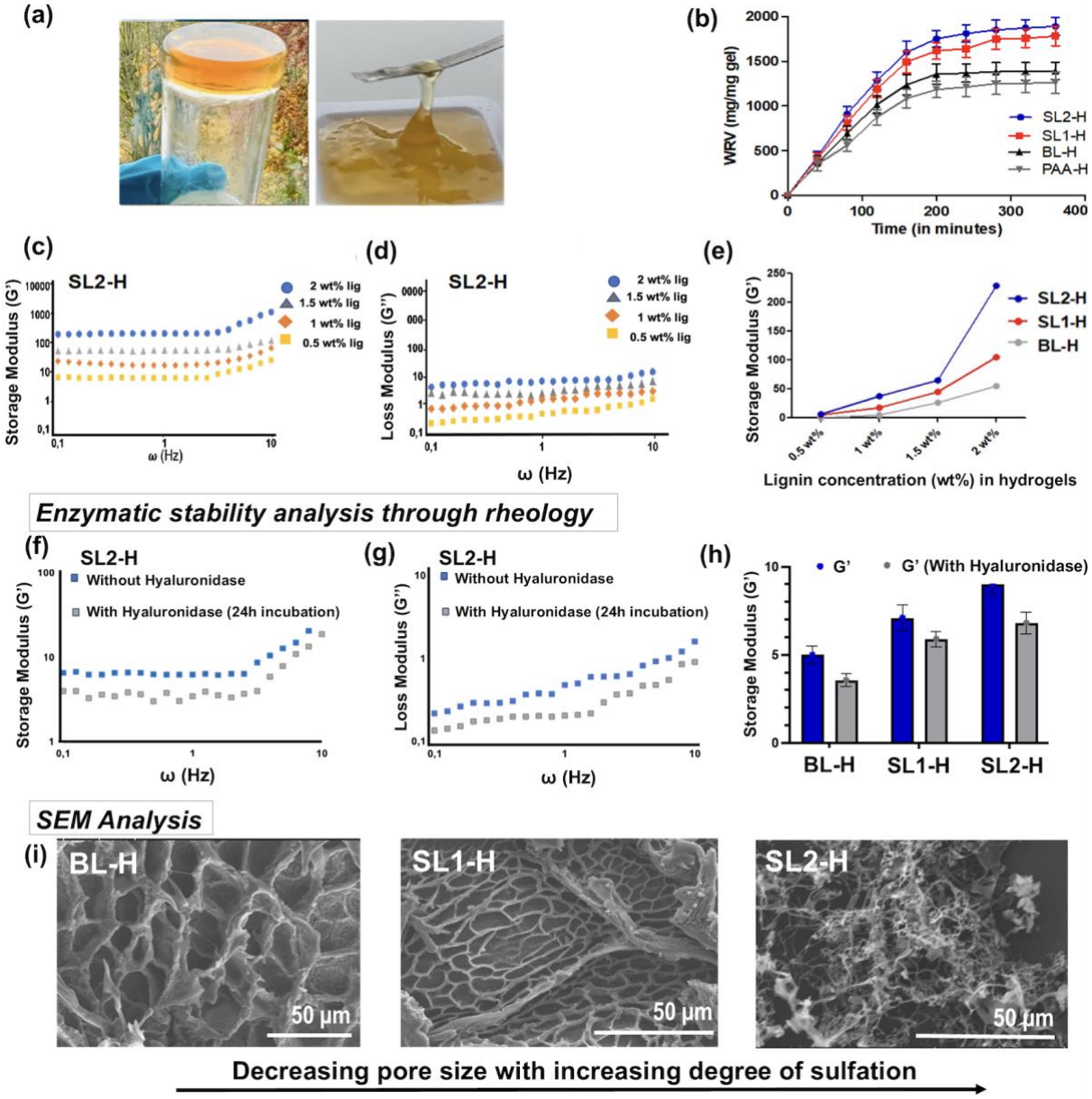

Figure 3. (a) Pictorial representation of the synthesized hydrogel (b) swelling capacity analysis of the bare and sulfated lignin hydrogels (c) Effect of the degree of sulfation on the storage modulus of the hydrogels (d) Storage Modulus of sulfated lignin at different concentrations (e) Loss Modulus of sulfated lignin at different concentrations (f)Effect of enzyme incubation on the storage modulus of hydrogels (g) Storage modulus plots of SL2-H after incubation with hyaluronidase (h) Loss Modulus plots of SL2-H after incubation with hyaluronidase (i) SEM analysis of bare lignin hydrogel (BL-H) and sulfated lignin hydrogels (SL1-H and SL2-H)

This observation was made at different weight concentrations of the hydrogel, which pointed towards the interesting possibility of tuning the pore size distribution of lignin hydrogels using the appropriate degree of functionalization, *i.e.*, sulfation. There are few reports on tuning the pore size distribution of hydrogels using variable concentrations of the precursor,[45] however the effect of the degree of functionalization of the precursor molecule on the mesh size of hydrogels

is still an unexplored area. This interesting finding can be utilized in different fields to tune the porosity of the hydrogels by varying the degree of functionalization of the precursor molecule.

Pathogen Binding: Inhibiting virus entry into the host cells at an early stage of infection is a promising concept for the prevention and treatment of infections. HSV-1 binds to the heparan sulfates on the host cell surface via its surface proteins gB and gC.[10, 46] It can be hypothesized that the presence of lignin functionalized with sulfate moieties competitively inhibits the virus due to multivalent binding of the glycan receptors to the sulfates on lignin (Figure 4a). The aqueous solutions of BL, SL1 and SL2 at different concentrations were incubated with HSV-1-GFP solution (200 plaque-forming units, PFU) for 45 minutes at room temperature. Then, the mixture was applied onto VeroE6 cells for 45 minutes at room temperature. After washing, the cells were infected with overlay medium (which has carboxymethyl cellulose (CMC) and ensures plaque formation) for 48 h at 37º C. As the virus has been modified with a green fluorescent protein (GFP) gene, infected cells express GFP for observation under the fluorescent microscope. Figure 4 shows the fluorescence microscopy images of the control as well as with the sulfated lignin at different concentrations. The cells were observed in the DAPI (blue) and GFP (green) channels, which enables quantifying the fraction of infected cells (GFP channel) across the entire cell ensemble (DAPI channel, staining the nucleus of cells). There were no plaques when the virus was pre-treated with the sulfated lignin, which gives proof of complete inhibition of the virus. Extracting dose-dependent inhibition bar graphs from this data indicated that increasing the degree of sulfation leads to higher inhibition by approximately 6 folds (Figure 4c and Table 1). It can be observed that SL2 shows the highest inhibition, followed by SL1 and BL. Here, the intrinsic antimicrobial activity of lignin (due to the presence of polyphenolic aromatic structure) can also play a certain role in the inhibitory activity of the BL. The IC_{50} values of BL, SL1, and SL2 were found to be 86.8, 2.9, and 0.5 µg/ml respectively (summarized above in Table 1).

Further, the HSV-1 binding to lignin-based hydrogels was investigated. For this, the BL-H, SL1-H, and SL2-H hydrogels were incubated with HSV-1 solutions for 1 h at 37 ºC. Afterwards, the number of infectious viruses in the supernatant was titrated on Vero E6 cells via plaque assay. The virus binding with hydrogels should result in a reduced virus titer in the supernatant (represented in Figure 4d). The sulfated lignin hydrogels exhibited much higher adsorption capacities than their non-sulfated counterparts. The concentration of sulfated lignin played an important role in the binding ability of the hydrogels, as the binding and inhibition of the viruses increased with an increase in the concentrations. The SL1-H and SL2-H present more virus binding sites, i.e. sulfate groups across their structures than BL-H, both in the case of hydrogels and hydrogel components, *i.e.*, lignin. It was clearly observed that complete adsorption of the HSV-1 occurred at a concentration of 1.5 wt% of SL1-H hydrogels and 1 wt% of SL2-H hydrogels. It can also be correlated with the increased cross-linking density and porous network of SL2-H as compared to SL1 and BL. Therefore, it can be concluded that the higher cross-linking within the hydrogels directly influences the pathogen binding, which leads to stronger inhibition of the pathogens.

Interestingly, the impact of DoS on the inhibition efficacy was much more pronounced for lignin-based hydrogels than it for non-crosslinked lignin: while the addition of sulfates to BL improved the inhibitory concentration by two orders of magnitude (BL vs. SL2, Figure 4c), a much stronger reduction of more than four orders of magnitude was found for the lignin-based hydrogels (BL-H vs. SL2-H, Figure 4d). This indicates that hydrogel formation indeed provides an advantage over the direct application of sulfated lignin. This observation might be attributed to an optimized 3D presentation of sulfated lignin within the hydrogel and motivates

further investigation on the impact of hydrogel structure and functionalization on pathogen retention.

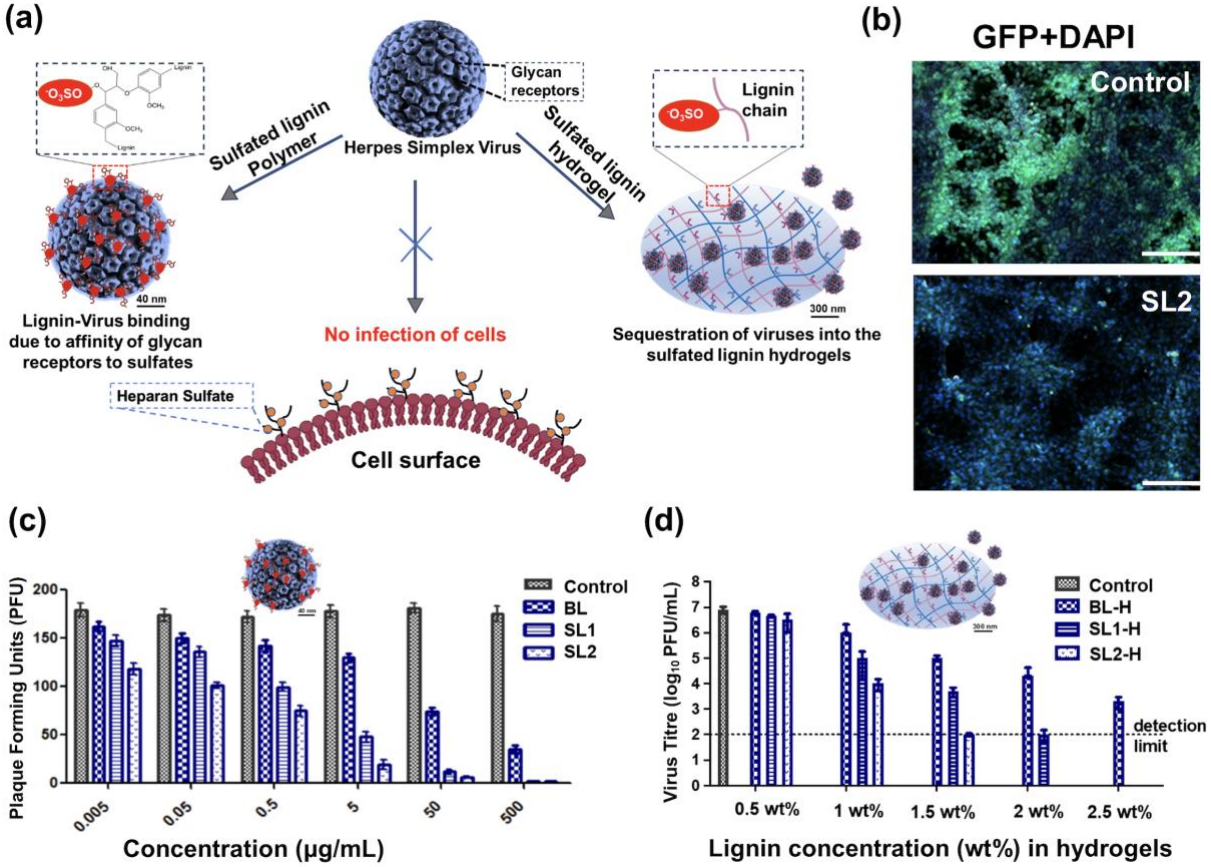

Figure 4. (a) Concept of HSV-1 inhibition through sulfated lignin (b) Initial qualitative examination of the HSV-1 inhibition through fluorescence microscopy at a scale of 200 µm (c) quantitative estimation of HSV-1 inhibition by lignin powders (d) quantitative estimation of HSV-1 inhibition by lignin hydrogels with different weight percentages of lignin

To assess for a potential broader spectrum of antimicrobial activity, we tested our compounds for activity against *E. coli* (Figure 5) and influenza A virus X31/H3N2 (Figure S10, supporting information). As we have seen that the hydrogel probably absorbs the HSV-1, it was speculated other microorganisms showed a similar effect. Interestingly, the sulfated lignin hydrogels reduced the virus infection for influenza A virus as well. The effect was, however, less pronounced in comparison to HSV-1 (Figure S10, supporting information). This inhibition effect could be attributed to the surface adsorption or adherence of the influenza A virus towards the lignin hydrogels. In contrast, the developed hydrogels were highly effective against *E. coli* bacteria, with a reduction of growth in solution as indicated by optical density measurements (Figures 5a) and of colony forming unit by more than 5 orders of magnitude (Figures 5b).

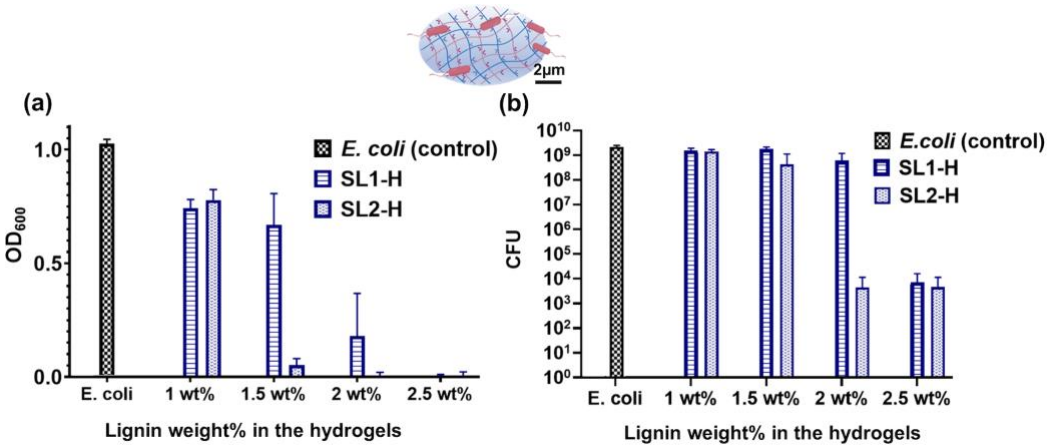

Figure 5. (a) Estimation of *E. coli* growth with optical density (OD) measurement of different hydrogel samples (b) Quantitative estimation of *E. coli* inhibition by lignin hydrogels

As the inhibition is more prominent only in the case of the sulfated lignin hydrogels (SL1-H and SL2-H), it can be speculated that the acidic behavior of the sulfated lignin hydrogels (due to the release of H^+ ions) can also be responsible for the inhibitory behavior of hydrogels along with the surface adherence of the pathogens. These experiments conclude that the sulfated lignin hydrogels can be applied to a broad spectrum of pathogens and hence, increase their applicability as mucus-mimicking hydrogels.

Experimental Details:

Sulfation of lignin: For the sulfation of lignin (Sigma-Aldrich/Merck, Cat Number 370959), sulfur trioxide pyridine complex was used. Lignin (400 mg) was mixed with sulfur trioxide pyridine complex (1.5 eq. w/w) in dry DMF (20 mL) at 60 °C for 20 h under argon atmosphere. After the reaction time was over, the pH value was increased to pH 10 by the addition of sodium hydroxide solution (0.3 mol L^{-1}). The product was dialyzed against sodium hydroxide solution (0.3 mol L^{-1}), 10 wt% NaCl and then water to remove the unreacted components.

Characterization of the sulfated lignin: The yield of the sulfation was analyzed by elemental analysis. The molecular weight distribution of the bare and sulfated lignin (8 mg/mL) was determined by means of GPC coupled to a refractive index detector (RI) for obtaining the complete distribution (M_n, M_p, M_w, dispersity) of with a GPC consisting of an Agilent 1100 solvent delivery system with pump, manual injector, and an Agilent differential refractometer. The hydrodynamic diameter was measured by dynamic light scattering at a concentration of 1 mg mL^{-1} in PBS buffer using Zetasizer Nano series (λ = 532 nm) from Malvern Panalytical. Before the measurement all samples were subjected to sonication for 15 minutes in a bath sonicator. Temperature equilibration was done for 1 min at 25 °C. The measurements were performed for ten scans each 15 s and the mentioned values result from at least three measurements. The surface charge was investigated by zeta-potential measurement with Zetasizer Nano series (λ = 532 nm) using folded capillary zeta cells (DTS 1070).

Dynamic Light Scattering and Zeta Potential Analysis: For measuring the hydrodynamic diameter and the surface charge, dynamic light scattering (DLS) was performed at a concentration of 0.3 mg mL^{-1} in deionized water using Zetasizer Nano series from Malvern

Panalytical. Disposable cuvettes (ZEN0040) made of polystyrene were used from Brand All the samples were sonicated for 15 minutes before the measurement. Temperature equilibration was done at 25 °C for 1 min. The measurements were performed for ten scans each 15 s in back scattering mode (173°). The average values resulting from at least three measurements were recorded. For the surface charge analysis, folded capillary zeta cells (DTS 1070) were procured from Malvern Panalytical. The average values resulting from five measurements with ten scans (each 15 s) were recorded to obtain the zeta potential for SL2, SL1 and BL.

NMR Analysis: NMR experiments were performed on a 500 MHz NMR spectrometer system (VNMRS500, Varian Associates, Palo Alto, USA) operating at proton frequency of 499.9 MHz (^{31}P-NMR at 202.4 MHz), which was equipped with a 5 mm OneNMR probe.
Gravimetry was performed on an ultramicrobalance (XP2 U/M, Mettler-Toledo, Gießen, Germany). Sample material, internal standard N-Hydroxy-5-norbornene-2,3-dicarboxylic acid imide (e-HNDI) and relaxation agent $Cr(acac)_3$ were accurately weighed and dissolved in the solvent mixture of $CDCl_3$/Pyridine 1:1.6 (v/v). Derivatization was performed as described in literature by adding 100 µL of 2-Chloro-4,4,5,5-tetramethyl-1,3,2-dioxaphospholane (TMDP) to the sample, followed by shaking it for ~ 1 h.[47] Samples SL1 and SL2 show incomplete solubility, only soluble phase was assessed by the NMR measurements for comparison. ^{31}P-NMR spectra on each sample were acquired accumulating 256 scans at a pulse angle of 90° and a relaxation delay of 10 s.

Gel permeation chromatography (GPC): A GPC system with WinGPC UniChrom 8.2 software (PSS GmbH) was used for the GPC analyses. The system was operated with an isocratic pump (HPLC COMPACT PUMP 3350, Bischoff) with a flow rate of 0.5 mL/min. DMSO (HPLC grade) was used as eluent with a salt addition of 0.075 M $NaNO_3$. A combination of four columns was used. At first a pre-column (ABOA DMSO-Phil-P-250, 8 mm x 50 mm, 10^2 – $7{\cdot}10^4$ g/mol, AppliChrom) was used followed by two columns (DMSO-Phil-P-250, 8 mm x 300 mm, 10^2 – $7{\cdot}10^4$ g/mol, AppliChrom) and final separation column (DMSO-Phil-P-Multipore, 15 µm, 8 mm x 300 mm, 10^2- 10^6 g/mol, AppliChrom). A column oven heated the separation columns to 60 °C (Thermostated Column Compartment). A refractive index detector (Shodex RI-501) and a photodiode array detector (SPD-M20A, Shimadzu Europe) were used to detect the fractions. The wavelength detector was operated at 280 nm. For calibration 10 pullulan standards (PSS GmbH, now Agilent) were used. Samples of 2-3 mg/ml concentration were filtered through a 0.2 µm syringe filter before injection.

Cell Viability Test: Vero E6 cells (Leibnitz Institute DSMZ – German Collection of Microorganisms and Cell Cultures GmbH) were routinely cultured in DMEM supplemented with 10% FBS and 1% Penicillin-Streptomycinat 37°C and 5% CO_2. For the viability test, 100µL per well of a 100000 cells/mL suspension in medium were seeded into white 96-well plates and incubated overnight. The next day, the test compounds were solubilized to a concentration of 10 mg/mL in Milli-Q H_2O or DMSO. Then, the compounds were further diluted in cell medium as a 10-fold serial dilution starting with the highest concentration of 1mg/mL. For the sample solubilized in DMSO, a control containing only DMSO, diluted in medium at the same percentages as used for the sample, was included. The supernatant of the cells was removed and replaced with 100µL/ well of the different compound dilutions in the medium. After 48h of incubation, the supernatant was removed and replaced with 50µl / well fresh medium and 50µL/well CellTiter-Glo® Reagent, which was prepared according to the instructions of the manufacturer (CellTiter-Glo® Luminescent Cell Viability Assay, Promega). Well contents were mixed for 2 minutes on a shaker, incubated at room temperature for 30 min and the luminescent signal was measured in a SPARK® multimode microplate

reader (Tecan). All tests were prepared 3 times independently in duplicates. Average values of the test wells were calculated, divided by the average values of untreated cells and expressed as % viability +/- standard deviation.

Synthesis of lignin hydrogels: Aqueous sulfated lignin solutions were prepared in various concentrations (0.5 to 2 % w/v) This was followed by the addition of polyacrylic acid aqueous solution (2.8 % w/v) to the reaction mixture and stirring at room temperature at a speed of 300 rpm for 5 min. Finally, ammonium persulfate (APS) (3% w/v) was added to the reaction mixture for the initiation of free radical generation, which mediated the cross-linking and co-polymerization between lignin and polyacrylic acid through formation of ester linkages. The reaction vials were then transferred to an incubator and left undisturbed at 70 °C for 20 min. After cooling down to room temperature, the lignin-based hydrogels were dialyzed with PBS for ~12 h using a 1 kD membrane. This facilitates the removal of unreacted APS and other contaminants.

Analysis of the swelling capacity of hydrogels: The hydrogels were immersed in deionized water. At each time interval, swelling gels were withdrawn from the solution and weighed out after removing the excess liquid from the gel surface. The excess water (or salt solution) was removed by filtration. The free swell water retention value (WRV), a measure of the dynamic water absorption properties of the gel, was calculated using the following equation:

$$\mathrm{WRV} = (Wt - W\mathrm{d})/W\mathrm{d} \times 100$$

where Wt is the weight of the wet gel at time t and Wd is the weight of the dried gel.

Enzyme degradation studies: The filtered enzyme solution was aliquoted and frozen at -20°C. Then, 500 µl of hydrogels are pipetted into 2 ml Eppendorf tubes using cut tips (200 µl), also known as 'wide bore'. This was followed by the addition of 100 µl of the enzyme solution/PBS to the tubes and thorough mixing by pipetting. The viscosity of the samples was measured directly, after 24 hours at 37°C. The samples are temporarily stored at 37°C without shaking.

Virus propagation and titration: HSV-1-GFP virus was kindly provided by Prof. Dr. Benedikt Kaufer and Prof. Dr. Klaus Osterrieder in Freie Universität Berlin. The virus was propagated on Vero E6 cells. Briefly speaking, the Vero E6 cells were seeded in T75 flask and were >90% confluency for the infection. Then the cells were infected by HSV-1-GFP at MOI 0.1 for 2 days in DMEM medium (with 10% FBS, Penti/strep). Then the cell culture supernatant was collected and centrifuged at 1000rpm for 10min. The supernatant after centrifugation was aliquoted and stored at -80°C. The virus stock was titrated by plaque assay on Vero E6 cells using MEM medium containing either 0.9% methycellulose or 0.6% Avicel (90% microcrystalline cellulose/10% carboxymethycellulose) as the overlay. After being fixed, the plaques can be counted by either under a fluorescent microscope or by eye after crystal violet staining.

Plaque reduction assay: the compounds were diluted 10-fold in 100 µL infection medium and then 100 µL of approx. 4000PFU/ml HSV-1-GFP dilution was added to the sample and incubated for 45min at r.t. Then 100µL of the virus was added onto Vero E6 cells and incubated

at r.t. with moderate shaking for 45min. Finally, the cells were washed with PBS once and then infected with the overlay medium for 2-4 days for plaque development. The plaques were counted as mentioned above.
Virus binding assay: The samples (5 µL each) were subjected to incubation with 100µL HSV-1-GFP solution (approx. 1×10^6 PFU/mL) for 1 hour. Then, the supernatant was collected and titrated by plaque assay on Vero E6 cells as described above. The binding with influenza A X31 virus was performed in the similar procedure, except that the virus in the supernatant was titrated on MDCK II cells as reported earlier.[48]

Fluorescence microscopy: After being fixed by 4% formaldehyde for 30 min, the cells were permeabilized with 0.1% Triton-X-100 in PBS at r.t. for 10 minutes, followed by washing once with PBS. Afterwards, DAPI (10 µg/ml) was added to stain the cell nuclei for 10 minutes. The cells were then washed with PBS, and the images were acquired with fluorescence microscope (Axio Z1, Zeiss, Germany).

In vitro antibacterial activity via growth curves and CFU assays: The K-12 derivative *E. coli* AR3110 was streaked out on LB agar from frozen stock. Single-colony was used to create the liquid culture that was grown to an OD_{600} of 0.600-0.800 at 37°C in LB media, shaking. The culture was then diluted in LB to a final OD_{600} concentration of 0.01, and 100 µL of this culture was added to 100 µL of UV-sterilized hydrogel of varying concentrations in a 96-well plate (round bottom, Sarstedt). Each well was thoroughly mixed by pipetting. The lid of the 96-well plate was coated in anti-fog solution (0.05% TritonX-100, 20% Ethanol in water[49] and allowed to completely dry under the clean bench hood. The closed with lid 96-well plate was placed in the Agilent BioTek Epoch 2 Microplate Spectrophotometer and allowed to grow for 20 hours at 37°C with continuous shaking (double orbital) measuring at OD_{600} in 15 min intervals. The OD_{600} after 20 hours was used for graph generation. Three biological replicates were performed consisting each of three technical replicates. Error bars represent ±SD. Statistical analysis was executed using the GraphPad Prism software.

Colony forming units (CFUs) were then counted after the 20-hour growth curve using the resultant culture as described in Maan *et al.*[50] Briefly, the culture was transferred to a 96-well plate and a serial dilution from 10^0 to 10^{-7} was performed in DPBS. 20 µL of varying dilutions were spotted onto LB agar plates and allowed to dry completely in clean bench hood. Plates were incubated overnight at 37°C and CFUs were then counted. Three biological replicates were performed consisting each of three technical replicates. Error bars represent ±SD. Statistical analysis was executed using the GraphPad Prism software.

Conclusion:

Lignin is a promising scaffold for the large-scale synthesis of biocompatible mucus-mimicking hydrogels that exhibit antimicrobial activity. Sulfating lignin is found to significantly improve its water solubility and its interaction with sulfate-binding viruses, such as HSV-1, which increases with increasing degree of sulfation. Tuning the concentration and degree of sulfation of the lignin in the hydrogel enabled to form lignin-based hydrogels that resembled native mucus with respect to the presentation of virus attachment factors and rheological properties. SEM analysis revealed that increasing the degree of sulfation decreased the mesh-size distribution by orders of magnitude, which provides a novel and interesting means to fine-tune

virus-hydrogel interactions. At the highest degree of sulfation (conversion of ~ 90% of the available hydroxyl groups), the mesh-size distribution is on the order of native mucus (hundreds of nm). The corresponding hydrogel shows a very efficient infection inhibition, as indicated by a reduction in plaque and colony forming units by more the 4 orders of magnitude. These experiments demonstrated that forming hydrogels from pathogen-binding inhibitors can provide a substantial benefit in infection inhibition (attributed here to an improvement in pathogen sequestration in comparison to the non-crosslinked inhibitor). Although the lignins were functionalized only with sulfates in this study, the high abundance of hydroxyl groups in lignin will enable for a feasible extension toward further pathogen attachment factors.

Acknowledgements:

The authors gratefully acknowledge financial support from the Deutsche Forschungsgemeinschaft (DFG, German Research Foundation) – Project ID 431232613 – SFB 1449 and Federal Ministry of Education and Research (BMBF). The authors would like to thank the Core Facility BioSupraMol for assistance with Elemental Analysis. SC would like to acknowledge the financial support from the Rising Star Fellowship, Freie Universität Berlin.

References:

(1) Beaucamp, A.; Muddasar, M.; Amiinu, I. S.; Leite, M. M.; Culebras, M.; Latha, K.; Gutiérrez, M. C.; Rodriguez-Padron, D.; del Monte, F.; Kennedy, T. Lignin for energy applications–state of the art, life cycle, technoeconomic analysis and future trends. *Green Chemistry* **2022**.
(2) Ji, D.; Park, J. M.; Oh, M. S.; Nguyen, T. L.; Shin, H.; Kim, J. S.; Kim, D.; Park, H. S.; Kim, J. Superstrong, superstiff, and conductive alginate hydrogels. *Nature Communications* **2022**, *13* (1), 3019.
(3) Bej, R.; Haag, R. Mucus-Inspired Dynamic Hydrogels: Synthesis and Future Perspectives. *Journal of the American Chemical Society* **2022**, *144* (44), 20137-20152. DOI: 10.1021/jacs.1c13547.
(4) Leal, J.; Smyth, H. D. C.; Ghosh, D. Physicochemical properties of mucus and their impact on transmucosal drug delivery. *Int J Pharm* **2017**, *532* (1), 555-572. DOI: 10.1016/j.ijpharm.2017.09.018 From NLM.
(5) McGuckin, M. A.; Lindén, S. K.; Sutton, P.; Florin, T. H. Mucin dynamics and enteric pathogens. *Nature Reviews Microbiology* **2011**, *9* (4), 265-278. DOI: 10.1038/nrmicro2538.
(6) Yang, S.; Duncan, G. A. Synthetic mucus biomaterials for antimicrobial peptide delivery. *Journal of Biomedical Materials Research Part A* **2023**.
(7) Campbell, K. T.; Wysoczynski, K.; Hadley, D. J.; Silva, E. A. Computational-based design of hydrogels with predictable mesh properties. *ACS biomaterials science & engineering* **2019**, *6* (1), 308-319.
(8) Lieleg, O.; Lieleg, C.; Bloom, J.; Buck, C. B.; Ribbeck, K. Mucin Biopolymers As Broad-Spectrum Antiviral Agents. *Biomacromolecules* **2012**, *13* (6), 1724-1732. DOI: 10.1021/bm3001292.

(9) Zanin, M.; Baviskar, P.; Webster, R.; Webby, R. The Interaction between Respiratory Pathogens and Mucus. *Cell Host & Microbe* **2016**, *19* (2), 159-168. DOI: https://doi.org/10.1016/j.chom.2016.01.001.
(10) Sharma, A.; Thongrom, B.; Bhatia, S.; von Lospichl, B.; Addante, A.; Graeber, S. Y.; Lauster, D.; Mall, M. A.; Gradzielski, M.; Haag, R. Polyglycerol-Based Mucus-Inspired Hydrogels. *Macromolecular Rapid Communications* **2021**, *42* (20), 2100303.
(11) Yan, H.; Melin, M.; Jiang, K.; Trossbach, M.; Badadamath, B.; Langer, K.; Winkeljann, B.; Lieleg, O.; Hong, J.; Joensson, H. N. Immune-Modulating Mucin Hydrogel Microdroplets for the Encapsulation of Cell and Microtissue. *Advanced Functional Materials* **2021**, *31* (42), 2105967.
(12) Abdel Aziz, M. H.; Mosier, P. D.; Desai, U. R. Identification of the site of binding of sulfated, low molecular weight lignins on thrombin. *Biochemical and Biophysical Research Communications* **2011**, *413* (2), 348-352. DOI: https://doi.org/10.1016/j.bbrc.2011.08.102.
(13) Afewerki, S.; Wang, X.; Ruiz-Esparza, G. U.; Tai, C.-W.; Kong, X.; Zhou, S.; Welch, K.; Huang, P.; Bengtsson, R.; Xu, C.; et al. Combined Catalysis for Engineering Bioinspired, Lignin-Based, Long-Lasting, Adhesive, Self-Mending, Antimicrobial Hydrogels. *ACS Nano* **2020**, *14* (12), 17004-17017. DOI: 10.1021/acsnano.0c06346.
(14) Mennani, M.; Kasbaji, M.; Benhamou, A. A.; Boussetta, A.; Mekkaoui, A. A.; Grimi, N.; Moubarik, A. Current approaches, emerging developments and functional prospects for lignin-based catalysts–Review. *Green Chemistry* **2023**.
(15) Wan, Y.; He, J.; Zhang, Y.; Chen, E. Y. X. One-Step Synthesis of Lignin-Based Triblock Copolymers as High-Temperature and UV-Blocking Thermoplastic Elastomers. *Angewandte Chemie* **2022**, *134* (8), e202114946.
(16) Malyar, Y. N.; Kazachenko, A. S.; Vasilyeva, N. Y.; Fetisova, O. Y.; Borovkova, V. S.; Miroshnikova, A. V.; Levdansky, A. V.; Skripnikov, A. M. Sulfation of wheat straw soda lignin: Role of solvents and catalysts. *Catalysis Today* **2022**, *397-399*, 397-406. DOI: https://doi.org/10.1016/j.cattod.2021.07.033.
(17) Levdansky, A. V.; Vasilyeva, N. Y.; Malyar, Y. N.; Kondrasenko, A. A.; Fetisova, O. Y.; Kazachenko, A. S.; Levdansky, V. A.; Kuznetsov, B. N. An Efficient Method of Birch Ethanol Lignin Sulfation with a Sulfaic Acid-Urea Mixture. *Molecules* **2022**, *27* (19), 6356.
(18) Zhang, C.; Shen, X.; Jin, Y.; Cheng, J.; Cai, C.; Wang, F. Catalytic strategies and mechanism analysis orbiting the center of critical intermediates in lignin depolymerization. *Chemical Reviews* **2023**, *123* (8), 4510-4601.
(19) Sharma, V.; Tsai, M.-L.; Nargotra, P.; Chen, C.-W.; Sun, P.-P.; Singhania, R. R.; Patel, A. K.; Dong, C.-D. Journey of lignin from a roadblock to bridge for lignocellulose biorefineries: A comprehensive review. *Science of The Total Environment* **2023**, *861*, 160560.
(20) Sethupathy, S.; Morales, G. M.; Gao, L.; Wang, H.; Yang, B.; Jiang, J.; Sun, J.; Zhu, D. Lignin valorization: Status, challenges and opportunities. *Bioresource Technology* **2022**, *347*, 126696.
(21) Liu, M.; Han, B.; Dyson, P. J. Simultaneous generation of methyl esters and CO in lignin transformation. *Angewandte Chemie International Edition* **2022**, *61* (40), e202209093.
(22) Agustiany, E. A.; Rasyidur Ridho, M.; Rahmi DN, M.; Madyaratri, E. W.; Falah, F.; Lubis, M. A. R.; Solihat, N. N.; Syamani, F. A.; Karungamye, P.; Sohail, A. Recent developments in lignin modification and its application in lignin-based green composites: A review. *Polymer Composites* **2022**, *43* (8), 4848-4865.

(23) Santo Pereira, A. d. E.; de Oliveira, J. L.; Savassa, S. M.; Rogério, C. B.; de Medeiros, G. A.; Fraceto, L. F. Lignin nanoparticles: New insights for a sustainable agriculture. *Journal of Cleaner Production* **2022**, *345*, 131145.
(24) Hatakeyama, H.; Hatakeyama, T. Lignin Structure, Properties, and Applications. *Advances in Polymer Science* **2009**, *232*, 1-63.
(25) Liu, X.; Inda, M. E.; Lai, Y.; Lu, T. K.; Zhao, X. Engineered living hydrogels. *Advanced Materials* **2022**, *34* (26), 2201326.
(26) Yang, D. Recent advances in hydrogels. ACS Publications: 2022; Vol. 34, pp 1987-1989.
(27) Blache, U.; Ford, E. M.; Ha, B.; Rijns, L.; Chaudhuri, O.; Dankers, P. Y.; Kloxin, A. M.; Snedeker, J. G.; Gentleman, E. Engineered hydrogels for mechanobiology. *Nature Reviews Methods Primers* **2022**, *2* (1), 98.
(28) Joonaki, E.; Hassanpouryouzband, A.; Heldt, C. L.; Areo, O. Surface chemistry can unlock drivers of surface stability of SARS-CoV-2 in a variety of environmental conditions. *Chem* **2020**, *6* (9), 2135-2146.
(29) Connolly, S. A.; Jardetzky, T. S.; Longnecker, R. The structural basis of herpesvirus entry. *Nature reviews Microbiology* **2021**, *19* (2), 110-121.
(30) Pouyan, P.; Nie, C.; Bhatia, S.; Wedepohl, S.; Achazi, K.; Osterrieder, N.; Haag, R. Inhibition of Herpes Simplex Virus Type 1 Attachment and Infection by Sulfated Polyglycerols with Different Architectures. *Biomacromolecules* **2021**, *22* (4), 1545-1554.
(31) Thongrom, B.; Sharma, A.; Nie, C.; Quaas, E.; Raue, M.; Bhatia, S.; Haag, R. Scaffold Flexibility Controls Binding of Herpes Simplex Virus Type 1 with Sulfated Dendritic Polyglycerol Hydrogels Fabricated by Thiol-Maleimide Click Reaction. *Macromolecular Bioscience* **2022**, *22* (5), 2100507.
(32) Ahmadi, V.; Nie, C.; Mohammadifar, E.; Achazi, K.; Wedepohl, S.; Kerkhoff, Y.; Block, S.; Osterrieder, K.; Haag, R. One-pot gram-scale synthesis of virucidal heparin-mimicking polymers as HSV-1 inhibitors. *Chemical Communications* **2021**, *57* (90), 11948-11951.
(33) Nie, C.; Pouyan, P.; Lauster, D.; Trimpert, J.; Kerkhoff, Y.; Szekeres, G. P.; Wallert, M.; Block, S.; Sahoo, A. K.; Dernedde, J. Polysulfates Block SARS-CoV-2 Uptake through Electrostatic Interactions. *Angewandte Chemie International Edition* **2021**, *60* (29), 15870-15878.
(34) Kesimer, M.; Ehre, C.; Burns, K. A.; Davis, C. W.; Sheehan, J. K.; Pickles, R. J. Molecular organization of the mucins and glycocalyx underlying mucus transport over mucosal surfaces of the airways. *Mucosal immunology* **2013**, *6* (2), 379-392.
(35) Granata, A.; Argyropoulos, D. S. 2-Chloro-4,4,5,5-tetramethyl-1,3,2-dioxaphospholane, a Reagent for the Accurate Determination of the Uncondensed and Condensed Phenolic Moieties in Lignins. *Journal of Agricultural and Food Chemistry* **1995**, *43* (6), 1538-1544. DOI: 10.1021/jf00054a023.
(36) Bhattacharjee, S. DLS and zeta potential – What they are and what they are not? *Journal of Controlled Release* **2016**, *235*, 337-351. DOI: https://doi.org/10.1016/j.jconrel.2016.06.017.
(37) Lowry, G. V.; Hill, R. J.; Harper, S.; Rawle, A. F.; Hendren, C. O.; Klaessig, F.; Nobbmann, U.; Sayre, P.; Rumble, J. Guidance to improve the scientific value of zeta-potential measurements in nanoEHS. *Environmental Science: Nano* **2016**, *3* (5), 953-965.
(38) Kazachenko, A. S.; Akman, F.; Vasilieva, N. Y.; Malyar, Y. N.; Fetisova, O. Y.; Lutoshkin, M. A.; Berezhnaya, Y. D.; Miroshnikova, A. V.; Issaoui, N.; Xiang, Z. Sulfation of Wheat Straw Soda Lignin with Sulfamic Acid over Solid Catalysts. *Polymers* **2022**, *14* (15), 3000.

(39) Malyar, Y. N.; Vasil'yeva, N. Y.; Kazachenko, A. S.; Skvortsova, G. P.; Korol'kova, I. V.; Kuznetsova, S. A. Sulfation of Abies Ethanol Lignin by Complexes of Sulfur Trioxide with 1,4-Dioxane and Pyridine. *Russian Journal of Bioorganic Chemistry* **2020**, *47*, 1368 - 1375.
(40) Alam, M. N.; Christopher, L. P. Natural Cellulose-Chitosan Cross-Linked Superabsorbent Hydrogels with Superior Swelling Properties. *ACS Sustainable Chemistry & Engineering* **2018**, *6* (7), 8736-8742. DOI: 10.1021/acssuschemeng.8b01062.
(41) Lafforgue, O.; Seyssiecq, I.; Poncet, S.; Favier, J. Rheological properties of synthetic mucus for airway clearance. *Journal of Biomedical Materials Research Part A* **2018**, *106* (2), 386-396.
(42) Vinod, A.; Tadmor, R.; Katoshevski, D.; Gutmark, E. J. Gels That Serve as Mucus Simulants: A Review. *Gels* **2023**, *9* (7), 555.
(43) Petrou, G.; Crouzier, T. Mucins as multifunctional building blocks of biomaterials. *Biomaterials science* **2018**, *6* (9), 2282-2297.
(44) Wheeler, K. M.; Cárcamo-Oyarce, G.; Turner, B. S.; Dellos-Nolan, S.; Co, J. Y.; Lehoux, S.; Cummings, R. D.; Wozniak, D. J.; Ribbeck, K. Mucin glycans attenuate the virulence of Pseudomonas aeruginosa in infection. *Nature microbiology* **2019**, *4* (12), 2146-2154.
(45) Zhao, Z.; Das, S.; Zharnikov, M. Tuning the Properties of Poly(ethylene glycol) Films and Membranes by the Molecular Weight of the Precursors. *ACS Applied Polymer Materials* **2022**, *4* (1), 645-653. DOI: 10.1021/acsapm.1c01569.
(46) Shukla, D.; Spear, P. G. Herpesviruses and heparan sulfate: an intimate relationship in aid of viral entry. *The Journal of clinical investigation* **2001**, *108* (4), 503-510.
(47) Korntner, P.; Sumerskii, I.; Bacher, M.; Rosenau, T.; Potthast, A. Characterization of technical lignins by NMR spectroscopy: optimization of functional group analysis by 31P NMR spectroscopy. *Holzforschung* **2015**, *69* (6), 807-814.
(48) Bhatia, S.; Lauster, D.; Bardua, M.; Ludwig, K.; Angioletti-Uberti, S.; Popp, N.; Hoffmann, U.; Paulus, F.; Budt, M.; Stadtmüller, M.; et al. Linear polysialoside outperforms dendritic analogs for inhibition of influenza virus infection in vitro and in vivo. *Biomaterials* **2017**, *138*, 22-34. DOI: https://doi.org/10.1016/j.biomaterials.2017.05.028.
(49) Brewster, J. D. A simple micro-growth assay for enumerating bacteria. *Journal of microbiological methods* **2003**, *53* (1), 77-86.
(50) Maan, H.; Povolotsky, T. L.; Porat, Z.; Itkin, M.; Malitsky, S.; Kolodkin-Gal, I. Imaging flow cytometry reveals a dual role for exopolysaccharides in biofilms: To promote self-adhesion while repelling non-self-community members. *Computational and structural biotechnology journal* **2022**, *20*, 15-25.

TOC Graphics